# Delay Time Enhanced Photonic Crystal Fiber Array for Wireless Communications using 2-D X-band Phased Array Antennas

Yongqiang Jiang, Zhong Shi, Brie Howley, Xiaonan Chen, Maggie Y. Chen[1)], Ray T. Chen*
Microelectronic Research Center, Department of Electrical and Computer Engineering,
The University of Texas at Austin, 10100 Burnet Rd, PRC/MER 1.606G, Austin, TX 78758, USA
1) Omega Optics, 10435 Burnet Road, Suite 108, Austin, TX 78758
* Email: chen@ece.utexas.edu

## ABSTRACT

Continuously tunable optical true time-delay (TTD) modules based on dispersion enhanced photonic crystal fibers (DEPCFs) are demonstrated to provide continuous microwave squint-free beam scanning for an X-band (8-12GHz) phased array antenna (PAA) system. The dispersion of the fabricated photonic crystal fibers (PCFs) is as high as –600 ps/nm·km at 1550 nm. By employing PCFs to increase the dispersion, the TTD module size can be proportionally reduced. The time delay is continuously tunable from -31 picosecond to 31 picosecond between adjacent delay lines by tuning the laser wavelength continuously from 1528 nm to 1560 nm. The far field radiation patterns of a 1×4 subarray were measured from $-45^{o}$ to $45^{o}$ scanning angles. Squint-free operation is experimentally confirmed. Wavelength conversion is also demonstrated to confirm that time delay information can successfully transferred from one wavelength to the other without being changed, which is suitable to be implemented in 2-D phased array antenna systems. The true-time delay formation idea presented here is suitable for not only X-band, but also the other higher microwave frequencies, such as K-band.

**Keywords**: Photonic crystal fiber (PCF), phased array antenna (PAA), optical true time delay (TTD), wavelength conversion (WC), semiconductor optical amplifier (SOA), wavelength tuning, dispersion

## I. INTRODUCTION

Phased array antennas (PAAs) are a promising technology in modern civilian and military communication and targeting systems. PAA's have the advantage of high directivity, quick beam steering without physical movement and reduced weight when compared to dish antennas. However, the application of phased-array antennas is limited by conventional, intrinsically narrow-band electrical phase trimmers and bulky electrical true-time-delay (TTD) networks. The narrow-band phase trimmer technique introduces beam squint. Since the 1990's, there has been growing interest in optical TTD techniques with the exciting features of wide bandwidth, reduced system weight and size, and low electromagnetic interference when compared with electrical TTD techniques [1-5]. However, most of the optical TTD techniques require a large number of precisely time-delay matched optical elements such as lasers and optical delay segments. This usually results in a complex system design that may also suffer from large power losses, specialized component needs, instability, or inability to easily scale to real-world two-dimensional (2-D) arrays. Esman et al proposed a fiber-optic TTD technique using conventional dispersion compensating fiber (DCF) to meet these requirements [2]. However, the dispersion parameter D, of conventional DCF is of fairly small magnitude (D = -100 ps/nm·km), and therefore long fiber lengths are still needed in the TTD module to get the required time delay. If the fiber group velocity dispersion is increased, the total fiber length will be decreased proportionally.

Conventional single-mode fibers (SMFs), which are based on weakly guiding structures with doped silica, can be tailored to slightly increase the dispersion by increasing the refractive index difference between the core and cladding [6]. However, the dispersion cannot be changed significantly because of the small index variation across the transverse cross section of the fiber from doping. This shortcoming can be overcome by the employment of dispersion enhanced photonic crystal fibers (DEPCFs). Photonic crystal fibers (PCFs) have generated a lot of interest due to their unusual and attractive properties [6-13]. They are usually made of silica or polymer materials with a regular hexagonal array of sub-micrometer-sized air holes running along the axis of the fiber as a cladding. A defect, usually one or multiple missing holes, acts as core. The dispersion of the PCFs can be flexibly tailored by tuning the pitch ($\Lambda$) of the periodic array, the hole diameter (d) and the doping concentration (n) of the core, as shown in Fig. 1.

In this paper, we implement a novel optical TTD module using an array of DEPCFs. The TTD module is designed, fabricated and evaluated. The approach is based on DEPCFs reported herein and other commercially available components, and has potentially high reliability and stability, as it requires no physically moving parts and no critical optical alignments. The microwave phase as the function of microwave frequency is measured to verify that the time delay is independent of microwave frequency. The

wide instantaneous bandwidth of the TTD module is confirmed by measurements of the far-field patterns of the X-band (8-12 GHz) PAA at two X-band frequencies. The optical wavelength conversion based on cross-gain-modulation (XGM) in semiconductor optical amplifiers (SOAs) is also experimentally confirmed by transferring time delay information from one optical wavelength to the other. This could be implemented in a 2-D PAA system.

## II. 2-D WAVELENGTH TUNABLE PAA SYSTEM

As shown in Fig. 2(a), a TTD module is proposed using dispersion enhanced photonic crystal fiber (DEPCF) delay lines. Each line has the same nominal group delay but with slightly different net dispersion. This is easily constructed by connecting differing lengths of DEPCFs and non-zero dispersion shifted fibers (NZDSFs) (D ≈ 3 ps/nm·km around 1550nm). By tuning the optical wavelength the relative delay of the signals between the lines will change. For example, at the central tuning wavelength $\lambda_0$ all the time delays are matched by trimming the NZDSFs to the appropriate length. Thus, at $\lambda_0$ the main antenna beam will be directed broadside. At a wavelength $\lambda$ less (or greater) than $\lambda_0$, each of the fiber delay lines adds (or subtracts) a time delay proportional to the dispersion coefficient, D, and the length of DEPCFs. We also need to note that the dispersion parameter of DEPCFs is usually more than two orders of magnitude higher than that of NZDSFs. So we can disregard the dispersion of NZDSFs here. Thus the delay $\Delta t$ between adjacent delay lines is

$$\Delta t = \int_{\lambda_0}^{\lambda} D_{DEPCF}(\lambda)\Delta l_{DEPCF} d\lambda \qquad (1)$$

where $\Delta l$ is the difference of the lengths of DEPCFs between adjacent delay lines. This results in element phasing such that the main antenna beam is steered in dual directions besides the array normal direction by tuning optical wavelength. Because the relative phasing is formed by true time delay through the DEPCFs array, beam squint is eliminated and all microwave frequencies are radiated at the same angle. [2]

The proposed schematic of the 1-D 1×N and 2-D N×N wavelength tunable PAA system setup is shown in Fig. 2(b). In the 1-D wavelength tunable PAA system, an elevation-control tunable laser is modulated by an intensity modulator and the X-band RF signal comes from a microwave source. The modulated optical signals then pass through a 1×N optical power splitter. After the splitter the optical signals are injected into the DEPCFs based TTD module described above. After the appropriated time delay within the delay modules, the 1×N optical signals are converted into the corresponding electrical signals by 1×N photodiodes. The electrical signals are then connected to a 1×N phased array antenna head. By tuning the elevation wavelengths we can obtain a 1-D continuously tunable true-time delay. The 2-D wavelength tunable PAA system can be considered as two 1-D system plus a mid-stage wavelength conversion. After the mid-stage wavelength conversion by a semiconductor optical amplifier (SOA), the optical signals from the first stage are converted to the wavelength of the azimuth-control tunable laser. Wavelength conversion can eliminate optical/electrical/optical conversion loss [5,14]. Similar to the first stage, after wavelength conversion each optical channel is input to another TTD module after a second 1×N optical power splitter. The TTD modules in the second stage could be any dispersion based optical TTD modules, and are not limited to be DEPCFs based TTD modules. After obtaining appropriate time delays within the delay modules, the N×N optical signals are converted into the corresponding electrical signals by N×N photodiodes. The electrical signals are then connected to an N×N phased array antenna head. By tuning the elevation and azimuth wavelengths we can obtain the 2-D continuously tunable true-time delay.

So far we can see from the system description above, the proposed approach is based on fibers and other commercially available components and has potentially high reliability and stability as it requires no moving parts during operation. The complexity and cost of the whole system could be greatly reduced. By using DEPCFs instead of conventional dispersion compensation fibers, the dispersion is dramatically increased so that the total fiber length will be decreased significantly. This makes the optical TTD modules ultra-compact.

## III. PHOTONIC CRYSTAL FIBER DESIGN, FABRICATION AND CHARACTERIZATION

The transverse section of photonic crystal fibers (PCFs) consists of a regular hexagonal array of microscopic holes in silica glass, polymer or other materials that extend along the entire fiber length. There are one or several defects (missing holes with or without doping) located in the center of the regular hexagonal structure. We use a two-core PCF design to achieve high dispersion. The inner core is a doped silica rod instead of a missing hole, and the outer core is 12 concentric doped silica rods instead of missing

holes, as shown in Fig. 1. Both cores are doped to have higher refractive index than pure silica, but the refractive index of the inner core is greater than that of the outer core. This two-core PCF can support two supermodes, which are analogous to the two supermodes of a directional coupler [15]. These modes are nearly phase matched at 1550 nm. Close to the phase matching wavelength, the mode index of the PCF changes rapidly due to strong coupling between the two individual modes of the inner core and outer core. Due to strong refractive index asymmetry between the two cores, there is a rapid change in the slope of the wavelength variation of the fundamental mode index. This leads to a large dispersion around 1550 nm. The air hole structure helps not only to guide the mode, but also to increase the dispersion value.

The dispersion of PCFs can be calculated using the full vectorial plane-wave expansion (PWE) method, which is fast and accurate compared to other methods [7]. We simulate the PCFs by using Bandsolve$^{TM}$ software that is based on full vectorial PWE. Since our PCF design is not a perfect crystal without defects, we need to use a supercell having a size of N×N instead of a natural unit cell to implement the periodic boundary conditions [7, 12-13]. As shown in Fig. 3 an 8×8 supercell is used for simulation purposes. Here 8×8 meets the simulation convergence compared with a 9×9 supercell.

The group velocity dispersion or simply the dispersion parameter D(λ) of the guided mode of the PCF can be directly calculated from the modal effective index $n_{eff}(\lambda)$ of the fundamental mode over a range of wavelengths [13]

$$D(\lambda) = -\frac{\lambda}{c}\frac{d^2 n_{eff}(\lambda)}{d\lambda^2} \tag{5}$$

where the effective refractive index of the mode is given by $n_{eff} = \beta[\lambda, n_m(\lambda)]/k_0$, where β is the propagation constant and $k_0$ is the free-space wave number. The dispersion parameter, D(λ), of PCF is strongly related to the structure and refractive index perturbation, and can thus be changed to achieve the desired characteristics [6,11,13]. In our design, we use different doping concentrations, period Λ, and hole diameters $d_0$, $d_1$, $d_2$, $d_3$, as shown in Fig. 3, to tune the dispersion. Here $d_0$ and $d_2$ are the diameters of the inner and outer doped silica rods, respectively. And $d_1$ and $d_3$ are the diameters of the air holes. By tuning these parameters, we can obtain the large dispersion parameter, D, value that we desire. Two guided modes are shown in Fig. 4. The guided mode in (a) corresponds to the supermode that is guided in the inner core, while the guided mode in (b) corresponds to that in the outer core. Fig. 5 shows the theoretical simulation results of dispersion enhanced PCFs (DEPCFs) with differing parameters using the full vectorial PWE method. High dispersion of about D = –3300 ps/nm·km is obtained at 1560 nm.

The DEPCFs is fabricated using the stack-and-draw technique, where silica glass capillaries are stacked in a desired lattice array, fused together, and then drawn down to PCFs [7-9]. A scanning electron micrograph (SEM) image of the cross section is shown in Fig. 6. In order to obtain a value of the chromatic dispersion of the fabricated DEPCFs, we measured the time delay between optical wavelengths of $\lambda_o \pm 0.1$ nm. To obtain the time delay, we measured the phase difference as a function of microwave frequency at optical wavelengths of ($\lambda_o$ + 0.1 nm) and ($\lambda_o$ - 0.1 nm). The time delay can be derived from the slope of each curve. The fiber chromatic dispersion is defined as $D = \Delta T/(\Delta\lambda \cdot L)$ which is obtained from the time delay divided by the fiber length and laser wavelength difference, 0.2 nm. The dispersion is –600 ps/nm·km at 1550 nm, as shown in Fig. 7. The dispersion is increased by 33 times compared to telecom SMF-28 that has a dispersion parameter of 18 ps/nm·km, and by 6 times compared to conventional dispersion compensation fiber (DCF).

## IV. TTD MODULE DESIGN, ASSEMBLY AND CHARACTERIZATION

A 1×4 TTD module is designed and assembled using the previously described dispersion enhanced photonic crystal fiber (DEPCF) and non-zero dispersion shifted fibers (NZDSFs), Lucent TrueWave SMF (D ≈ 3 ps/nm·km from 1530nm to 1565nm) as delay lines. The lengths of the DEPCFs are 10.500m (delay line #3), 7.000m (#2), 3.500m (#1) and 0m (#0), and the lengths of the non-zero dispersion shifted fibers (NZDSFs) are 0m, 3.500m, 7.000m, 10.500m, respectively, as shown in Fig. 2. The measured insertion losses of the delay lines are 3.4 dB, 3.3 dB, 3.2 dB, 0.5 dB, respectively. Each delay line has the same nominal group delay at the central tuning wavelength, $\lambda_0$ =1545 nm, but with slightly different net dispersion. Thus, at 1545 nm the main antenna beam will be directed broadside. At wavelengths deviating from 1545 nm, each fiber delay lines generates a time delay proportional to its dispersion parameter, D, and the DEPCF length.

The measured RF phase differences versus modulation frequency curves are shown in Fig. 8 for several wavelengths. The time delay shown in the inset is calculated from the slope of each curve. The1545 nm wavelength was chosen as a reference for zero time delay. By tuning the wavelength from 1528 nm to 1560 nm, time delays ranging from –31 ps to 31 ps between any two adjacent delay lines are achieved. This is equivalent to scanning angles ranging from $-45^o$ to $45^o$ for a 4-element PAA subarray having half-wavelength spacing at 10GHz. The linearity of phase versus frequency curve verifies the true-time delay and wide bandwidth capability of the proposed scheme.

## V. 1-D PAA SYSTEM MEASUREMENT

The assembled 4-element 1-D X-band PAA system which was described in section II is demonstrated. The experimental setup is shown in Fig. 9. An X-band (8-12 GHz) microwave signal is generated from an 8510C HP network analyzer [14]. The optical carrier from a tunable laser (tuning range: 1520-1580nm, spectral width: 200MHz, tuning resolution: <0.024nm) is modulated by a 10Gb/s $LiNiO_3$ modulator, optically amplified by an erbium doped fiber amplifier (EDFA), then distributed into the four TTD delay lines by a one-to-four fiber splitter. After the pre-determined time delay, the optical signals with the correct time delay relationships are detected by InGaAs high-speed photodiodes (bandwidth: 18 GHz) and individually fed into four antenna elements after electrical amplification. The microwave radiation signals are detected by an X-band receiving horn connected to a microwave spectra analyzer (MSA). A computer controlled rotational stage under the antenna head can rotate the antenna to measure the antenna radiation far field pattern.

Since the PAA elements emit most efficiently around the two frequencies of 9 and 10.3GHz, as seen from the plot of the S11 parameter of the phased array antenna in Fig. 10, the far field pattern of the PAA is measured at these two frequencies. Fig. 11 shows the far field patterns at $23^o$ scanning angle corresponding to a 17 ps delay time between adjacent delay lines using a laser wavelength of 1553 nm (compared to the reference wavelength of 1545 nm that results in $0^o$ scanning). From Fig. 11, it can be seen that the simulation results and measured data agree fairly well. The deviation from the theoretical prediction shown in Fig. 11 is due to non-uniformity between individual element radiation patterns. As expected, the measurement shows no beam squint effect.

We also need to mention that the ultimate application of this approach is also limited by the tuning speed of the tunable laser. Wipiejewski et al reports a tunable laser with 40ns tuning speed, which is fast enough for most PAA applications [16].

## VI. WAVELENGTH CONVERSION

In the 2-D PAA system, the signal can be converted from one optical wavelength to the other using a wavelength conversion technique. This could eliminate the optical/electrical/optical conversion loss and also make the system much more compact. Several techniques of wavelength conversion exist including cross-gain-modulation (XGM), cross-phase-modulation (XPM), and four-wave-mixing (FWM). In our experiment, we use wavelength conversion based on XGM in semiconductor optical amplifiers (SOAs) [5, 14,17]. By increasing input optical intensity, the gain of the SOA will saturate. Close to the saturation region of the SOA, an analog signal at optical wavelength $\lambda_1$ will modulate the gain of the SOA. Then a continuous wave (CW) beam at optical wavelength $\lambda_2$ will sample the gain modulation, thus copying the analog signal from $\lambda_1$ to $\lambda_2$, as shown in Fig. 12.

In order to make wavelength conversion work in the saturation region of the SOAs, we measured the gain versus input optical power curve with injection current of 150mA, as shown in Figure 13. The results shown in Fig. 13 experimentally confirmed the gain saturation.

In our 2-D PAA system, the purpose of wavelength conversion is to transfer the delay information from one optical wavelength to the other without alteration. In order to see if delay information has been changed after wavelength conversion, we measured the phase difference versus the modulation frequency in all 4 delay lines before wavelength conversion at $\lambda_{el}$ = 1550 nm and after wavelength conversion at $\lambda_{az}$ = 1542 nm (compared to the phase of the reference wavelength at $\lambda_{el}$ = 1545 nm). The block diagram of the measurement setup is shown in Fig. 14. We used the counter propagation scheme to save one optical filter [14]. We still set $\lambda_{el}$ = 1545 nm as reference wavelength with zero time delay. Before the wavelength conversion, the time delays in $\lambda_{el}$ = 1550 nm in delay line #3, #2, #1 and #0 are –31.1 ps, -20.6 ps, -10.3 ps, 0.2 ps, respectively, while after wavelength conversion the time delays at $\lambda_{az}$ = 1542 nm are –29.1 ps, -18.5 ps, -8.5 ps, 2.1 ps. The time delay of each delay line increases about 2 ps, but the delay difference between

adjacent delay lines still stays about the same. We can conclude that the time delay information is clearly transferred from elevation control to azimuth control through the wavelength conversion in the SOA.

## VII. CONCLUSION

A novel true-time delay module using dispersion enhanced photonic crystal fibers has been designed, fabricated, and experimentally evaluated in an X-band phased-array antenna system. This module is compact, low loss, and easy to package while providing wide instantaneous bandwidth. Squint-free operation is experimentally confirmed in a 1-D, 1×4 phased array antenna using this true time delay module. Wavelength conversion is demonstrated to transfer time delay information successfully from one wavelength to another, which is suitable for a 2-D phased array antenna system application.

## ACKNOWLEDGMENT

This research is supported by the Defense Advanced Research Project Agency (DARPA).

## REFERENCES

[1] W. Ng, A. A. Walston, G. L. Tangonan, J. J. Lee, I. L. Newberg, and N. Bernstein, "The first demonstration of an optically steered microwave phased array antenna using true-time-delay," IEEE Journal of Lightwave Technology, vol. 9, pp. 1124-1131, 1991

[2] R. D. Esman, M. Y. Frankel, J. L. Dexter, L. Goldberg, M. G. Parent, D. Stilwell, D. G. Cooper, "Fiber-optic prism true time-delay antenna feed", IEEE Photonics Technology Letter, vol. 11, pp. 1347-1349, 1993

[3] R. Soref, "Optical dispersion technique for time-delay beam steering", Appl. Opt. Vol. 31, pp. 7395-7397, 1992

[4] Y. Chen, R. T. Chen, "A fully packaged true time delay module for a K-band phased array antenna system demonstration", IEEE Photonics Technology Letters, vol. 14, pp. 1175 – 1177, 2002

[5] S. Yegnanarayanan, B. Jalali, "Wavelength-selective true time delay for optical control of phased-array antenna", IEEE Photonics Technology Letters, vol. 12, pp. 1049 – 1051, 2000

[6] L. P. Shen, W. P. Huang, G. X. Chen, S. S. Jian, "Design and optimization of photonic crystal fibers for broad-band dispersion compensation", IEEE Photonics Technology Letter, vol. 15, pp. 540-542, 2003

[7] A. Bjarklev, J. Broeng, A. Bjarklev, "Photonic Crystal Fibres", ISBN 1-4020-7610-X, Kluwer Academic Publishers, 2003

[8] P. St. J. Russell, "Photonic crystal fibers," Science, vol. 299, pp. 358-362, 2003

[9] J. A. West, N. Venkataramam, C. M. Smith, M. T. Gallagher, "Photonic crystal fibers", Proc. 27th Eur. Conf. on Opt. Comm. (ECOC '01), vol. 4, pp. 582 –585, 2001

[10] J. C. Knight, T. A. Birks, P. St. J. Russell, and D. M. Atkin, "All-silica single-mode optical fiber with photonic crystal cladding", Optics Letters, Vol. 21, pp. 1547-1549, 1996

[11] T. A. Birks, D. Mogilevtsev, J. C. Knight, P. St. J. Russell, "Dispersion compensation using single-material fibers", IEEE Photonics Technology Letters, vol. 11, pp. 674 – 676, 1999

[12] J. Broeng, S. E. Barkou, T. Sndergaard, A. Bjarklev, "Analysis of air-guiding photonic bandgap fibers", Opt. Lett., vol. 25, pp. 96-98, 2000

[13] A. Ferrando, E. Silvestre, J. J. Miret, P. Andrs, M. V. Andrs, "Full-vector analysisof a realistic photonic crystal fiber", Opt. Lett., vol. 24, pp. 276-278, 1999

[14] Z. Shi, B. Howley, Y. Jiang, etc, "True-time-delay modules based on single tunable laser in conjunction with waveguide-hologram for phased-array antenna application", Optical Engineering, in press, 2005

[15] K. Thyagarajan, R. K. Varshney, P. Palai, "A novel design of a dispersion compensating fiber", IEEE Photonic Technology Letters, vol. 8, pp. 1510-1512, 1996

[16] Y. Wipiejewski, Y. A. Akulova, C. Schow, "Monolithic Integration of a widely tunable laser diode with a high speed electro absorption modulator", Electronic Components and Technology Conference 2002, pp. 558-562, 2002

[17] M. Asghari, I. H. White, R. V. Penty, "Wavelength conversion using semiconductor optical amplifiers", vol. 15, pp. 1181-1190, 1997

## CAPTIONS

Fig.1. The layout of the transverse section of a model dispersion enhanced photonic crystal fiber.
Fig. 2. (a) Dispersion enhanced PCFs based wavelength continuously tunable TTD module. (b) Dispersion enhanced PCF based wavelength continuously tunable 1-D and 2-D PAA system structure. (Dashed line: dispersion enhanced PCF; solid line: Lucent TrueWave SMF; MOD: modulator; WC: wavelength conversion; PD: photodiode)
Fig. 3. Transverse section of a model dispersion enhanced PCF. The box with dimensions N×N corresponds to the supercell used to implement boundary conditions.
Fig. 4. Two guided modes of the dispersion enhanced PCF: (a) most mode energy in inner core, (b) most mode energy in outer core.
Fig. 5. Dispersion parameter D for dispersion enhanced PCF with various microstructure parameters.
Fig. 6. Scanning electron micrograph (SEM) image of the fabricated dispersion enhanced PCF.
Fig. 7. The simulated and measured chromatic dispersion parameter D for dispersion enhanced PCFs.
Fig. 8. Measured phase difference as a function of modulation frequency. The time delays between two adjacent delay lines are calculated from the slope of the phase versus microwave frequency.
Fig. 9. Picture of the X-band PAA system
Fig. 10. S11 of the X-band phased array patch antenna with two radiation peak frequencies at 9 and 10.3 GHz
Fig. 11. Comparison of far-field patterns of the PAA at $23^{o}$ scanning angle at frequencies of 9 and 10.3 GHz with an optical wavelength of 1553 nm.
Fig. 12. Mechanism of wavelength conversion from optical wavelength $\lambda_1$ to $\lambda_2$ by using cross gain modulation in the saturation region of semiconductor optical amplifiers
Fig. 13. The output gain as a function of different input optical power
Fig. 14. The block diagram of the experimental setup to measure the phase difference vs. modulation frequency after wavelength conversion in a semiconductor optical amplifier (MOD: modulator; EDFA: Erbium doped fiber amplifier; SOA: semiconductor optical amplifier; PD: photodiode; MSA: microwave spectra analyzer)
Fig. 15. Measured phase difference as a function of modulation frequency with the reference wavelength at $\lambda_{el}$ = 1545 nm. The time delays are calculated from the slope of the phase versus microwave frequency.

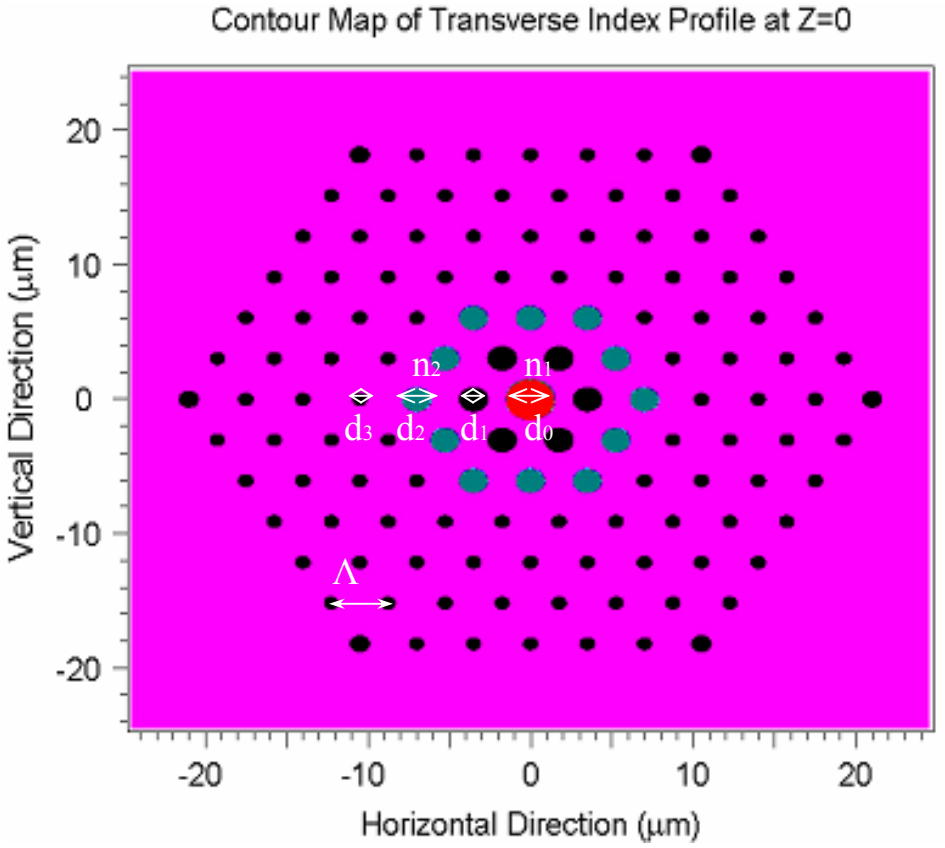
Contour Map of Transverse Index Profile at Z=0
Vertical Direction (μm)
Horizontal Direction (μm)
20
10
0
-10
-20
-20
-10
0
10
20
n2
n1
d3
d2
d1
d0
Λ

Fig.1

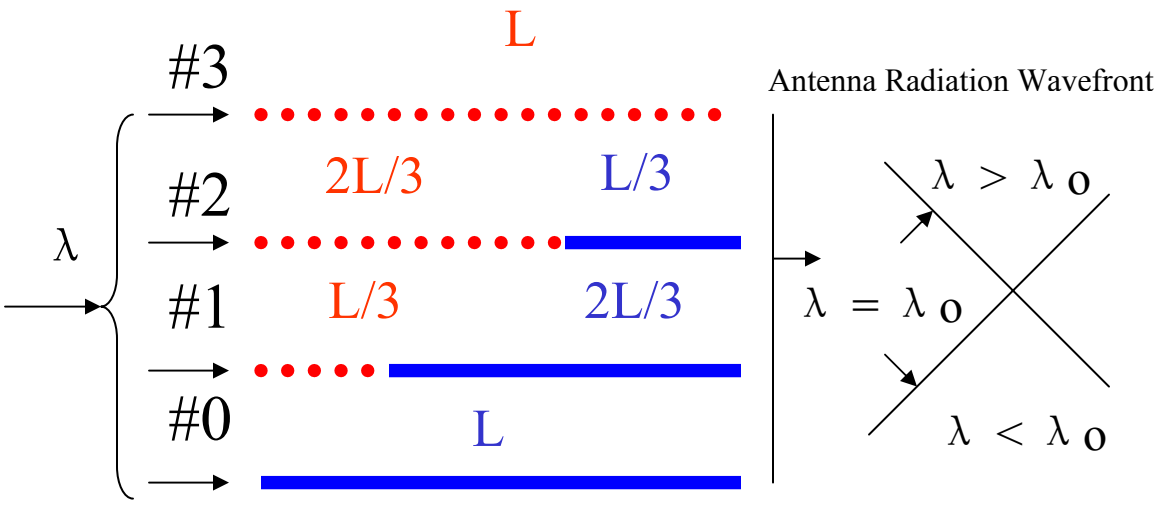
L
#3
#2
#1
#0
λ
2L/3
L/3
L/3
2L/3
L
Antenna Radiation Wavefront
λ > λ o
λ = λ o
λ < λ o

Fig. 2(a)

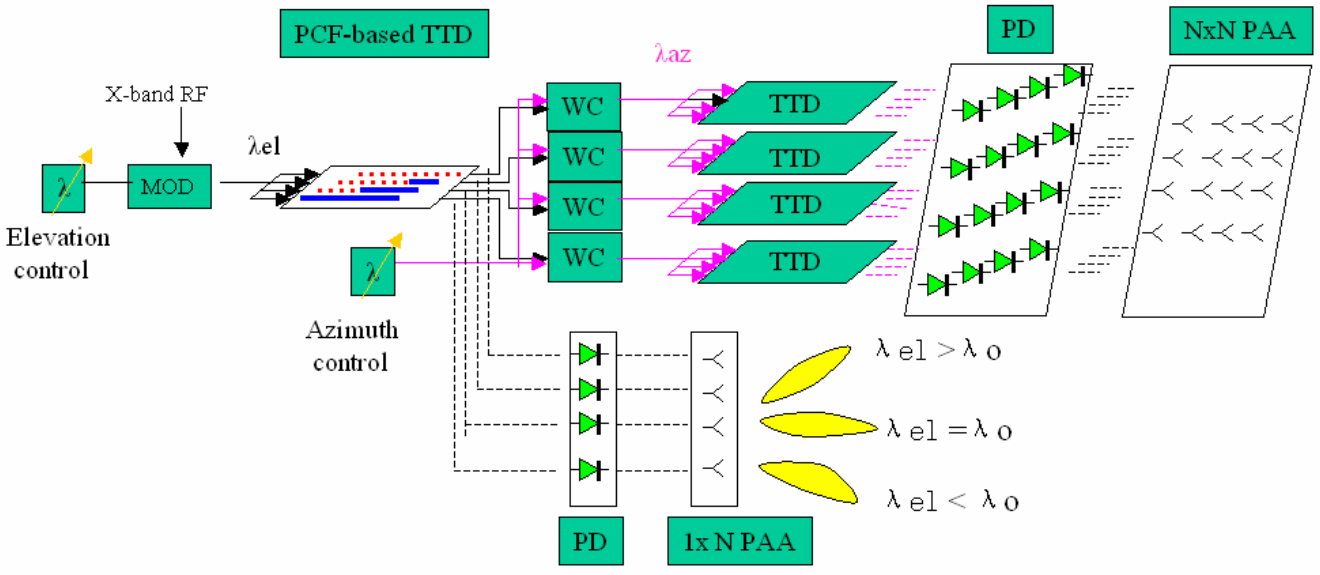
PCF-based TTD
X-band RF
MOD
λel
λaz
WC
WC
WC
WC
TTD
TTD
TTD
TTD
PD
NxN PAA
Elevation control
Azimuth control
λ el > λ o
λ el = λ o
λ el < λ o
PD
1x N PAA

Fig. 2(b)

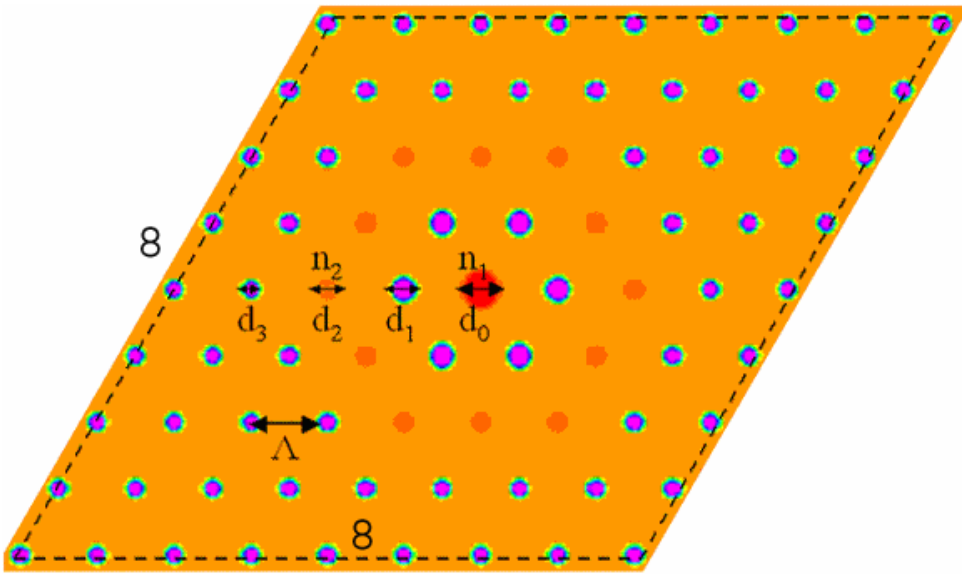
8
n2
n1
d3
d2
d1
d0
Λ
8

Fig. 3

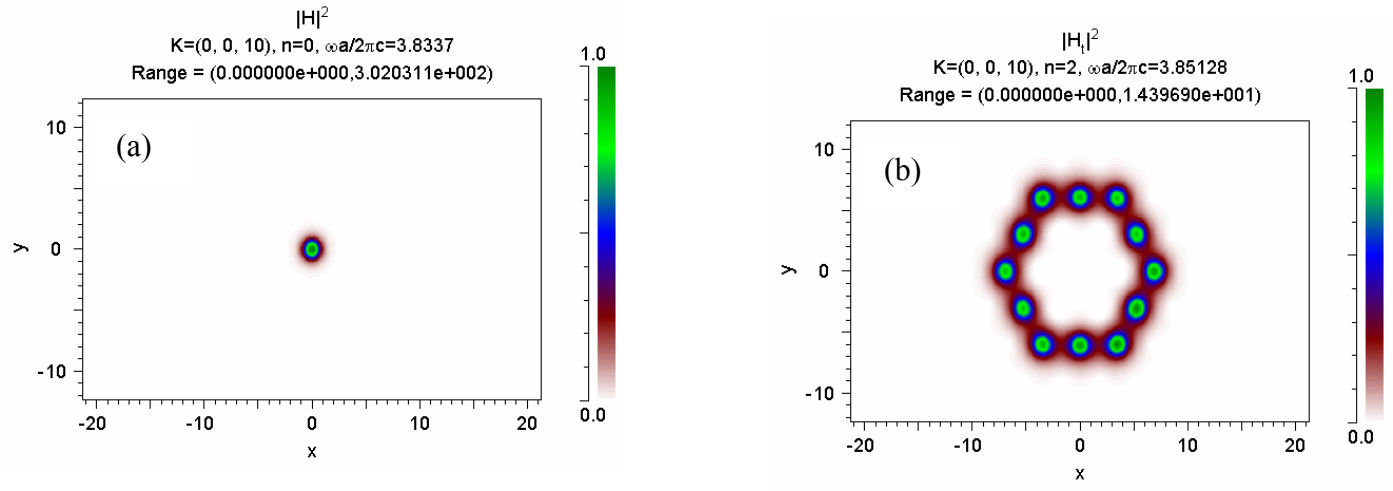
|H|2
K=(0, 0, 10), n=0, ωa/2πc=3.8337
Range = (0.000000e+000,3.020311e+002)
(a)
1.0
0.0
10
0
-10
-20
-10
0
10
20
x
y
|Ht|2
K=(0, 0, 10), n=2, ωa/2πc=3.85128
Range = (0.000000e+000,1.439690e+001)
(b)
1.0
0.0

Fig.4

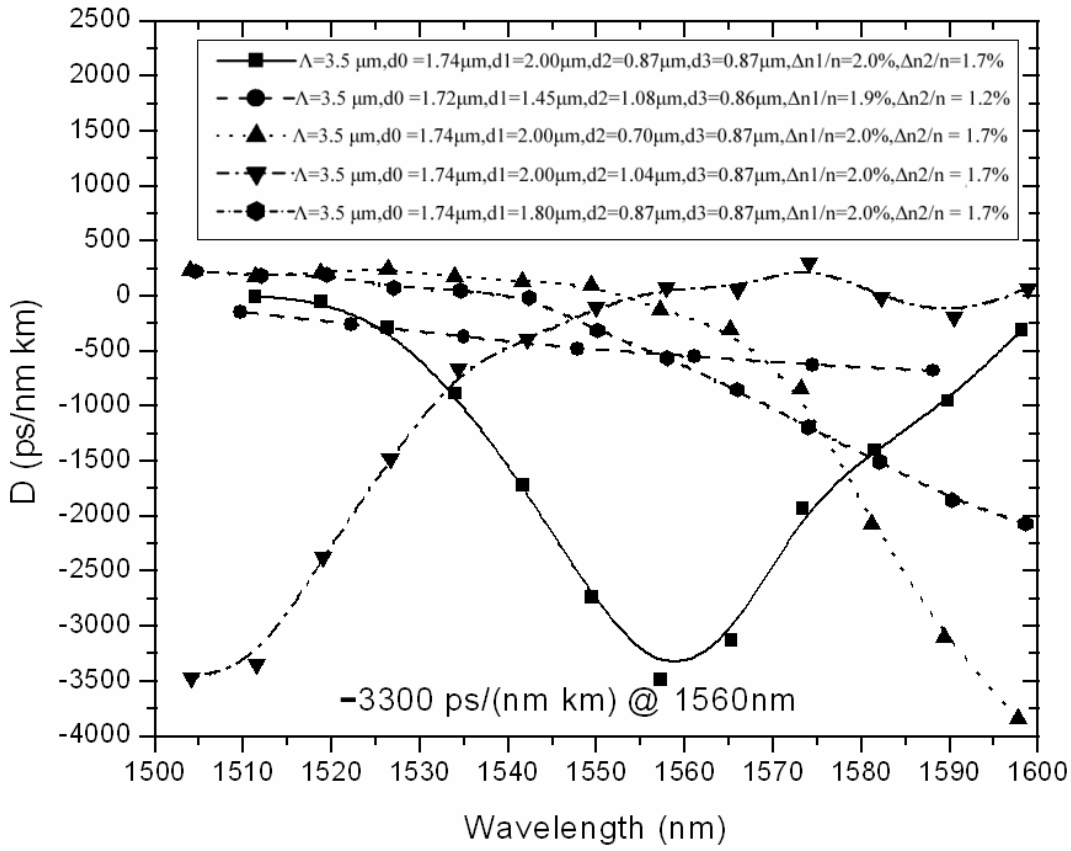
Λ=3.5 μm,d0 =1.74μm,d1=2.00μm,d2=0.87μm,d3=0.87μm,Δn1/n=2.0%,Δn2/n=1.7%
Λ=3.5 μm,d0 =1.72μm,d1=1.45μm,d2=1.08μm,d3=0.86μm,Δn1/n=1.9%,Δn2/n = 1.2%
Λ=3.5 μm,d0 =1.74μm,d1=2.00μm,d2=0.70μm,d3=0.87μm,Δn1/n=2.0%,Δn2/n = 1.7%
Λ=3.5 μm,d0 =1.74μm,d1=2.00μm,d2=1.04μm,d3=0.87μm,Δn1/n=2.0%,Δn2/n = 1.7%
Λ=3.5 μm,d0 =1.74μm,d1=1.80μm,d2=0.87μm,d3=0.87μm,Δn1/n=2.0%,Δn2/n = 1.7%
D (ps/nm km)
Wavelength (nm)
-3300 ps/(nm km) @ 1560nm

Fig. 5

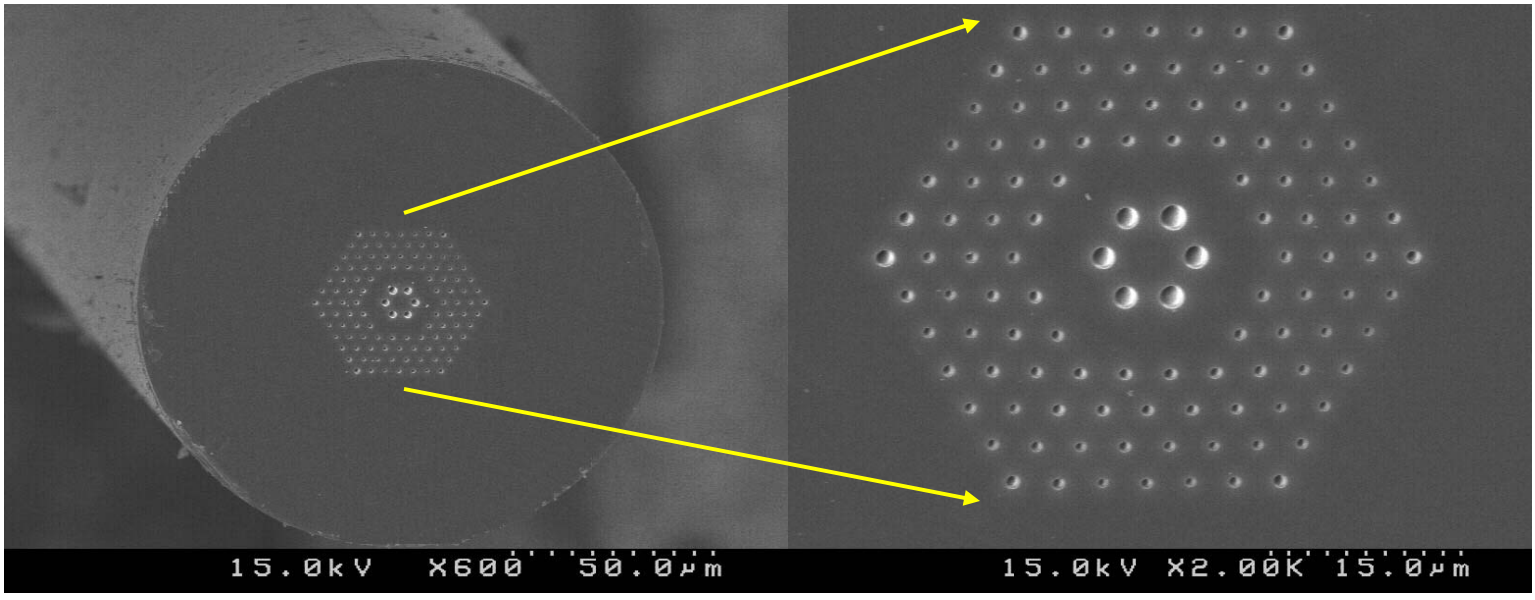
15.0kV X600 50.0μm
15.0kV X2.00K 15.0μm

Fig.6

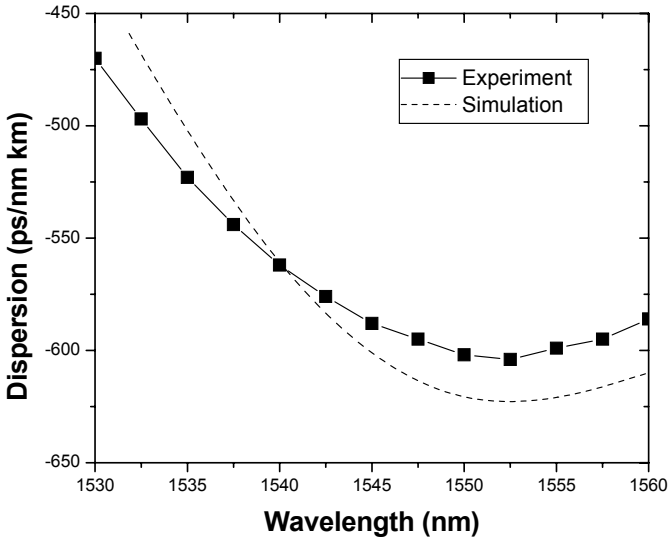
Experiment
Simulation
Dispersion (ps/nm km)
Wavelength (nm)
-450
-500
-550
-600
-650
1530
1535
1540
1545
1550
1555
1560

Fig.7

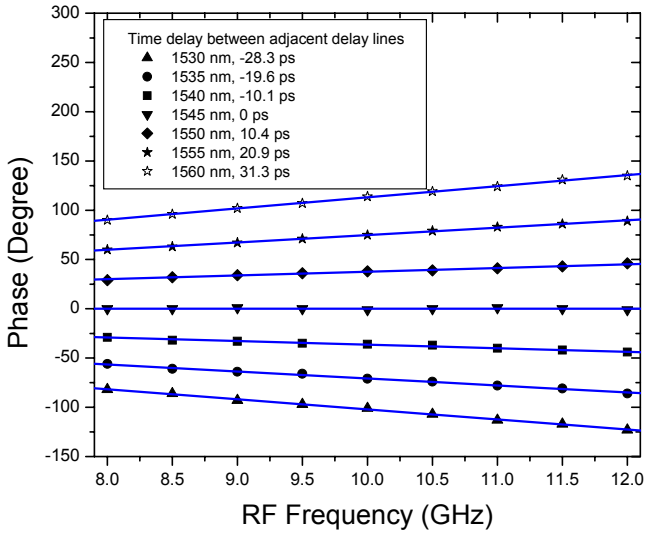
Time delay between adjacent delay lines
1530 nm, -28.3 ps
1535 nm, -19.6 ps
1540 nm, -10.1 ps
1545 nm, 0 ps
1550 nm, 10.4 ps
1555 nm, 20.9 ps
1560 nm, 31.3 ps
Phase (Degree)
RF Frequency (GHz)
300
250
200
150
100
50
0
-50
-100
-150
8.0
8.5
9.0
9.5
10.0
10.5
11.0
11.5
12.0

Fig. 8

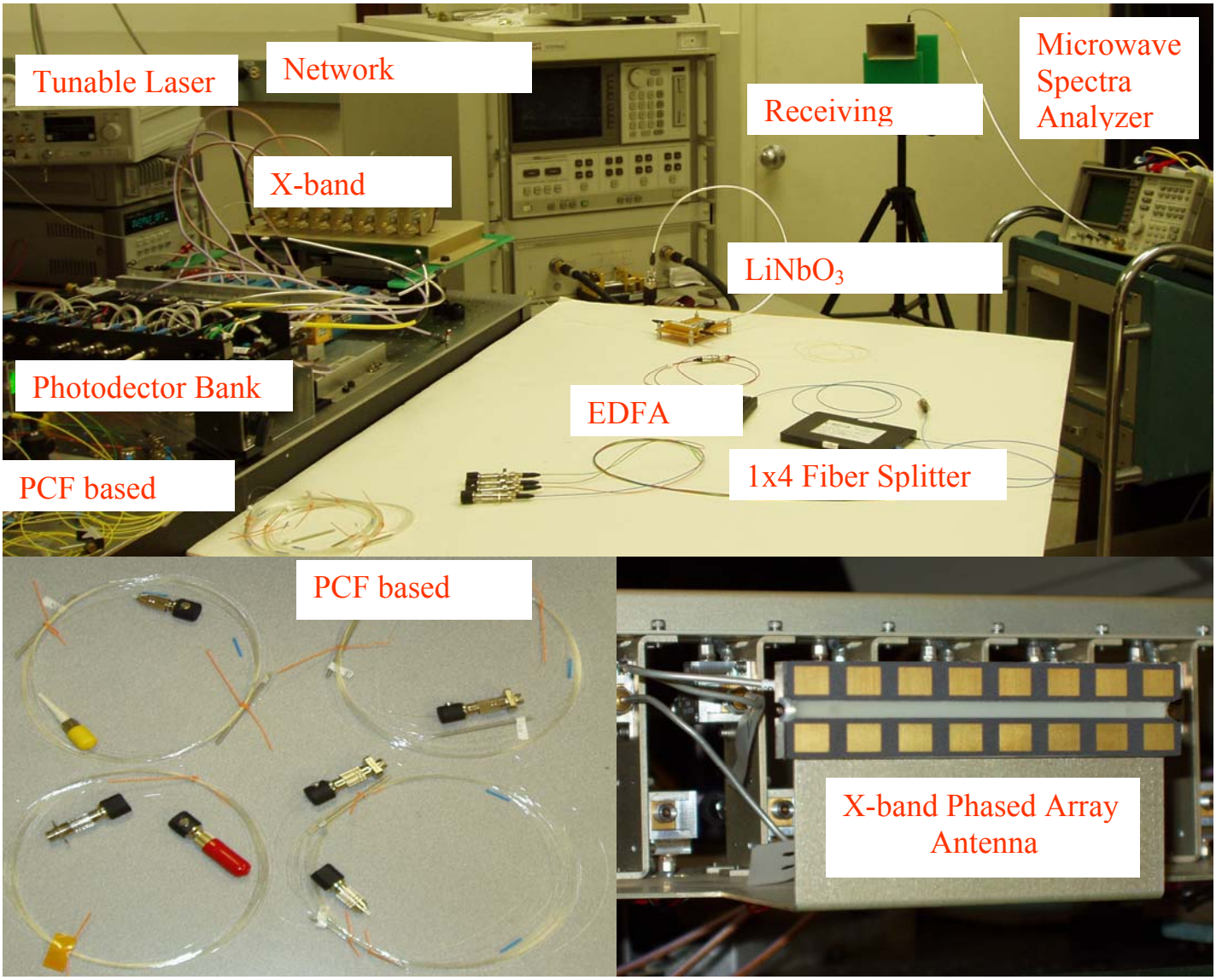
Tunable Laser
Network
Receiving
Microwave Spectra Analyzer
X-band
LiNbO3
Photodector Bank
EDFA
PCF based
1x4 Fiber Splitter
PCF based
X-band Phased Array Antenna

Fig. 9

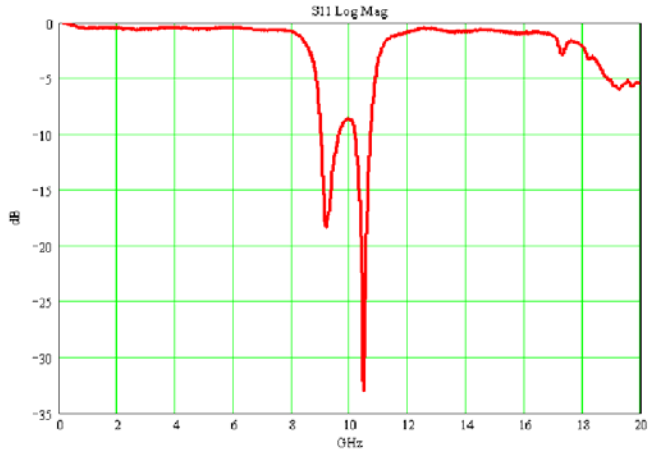
S11 Log Mag
dB
GHz

Fig. 10

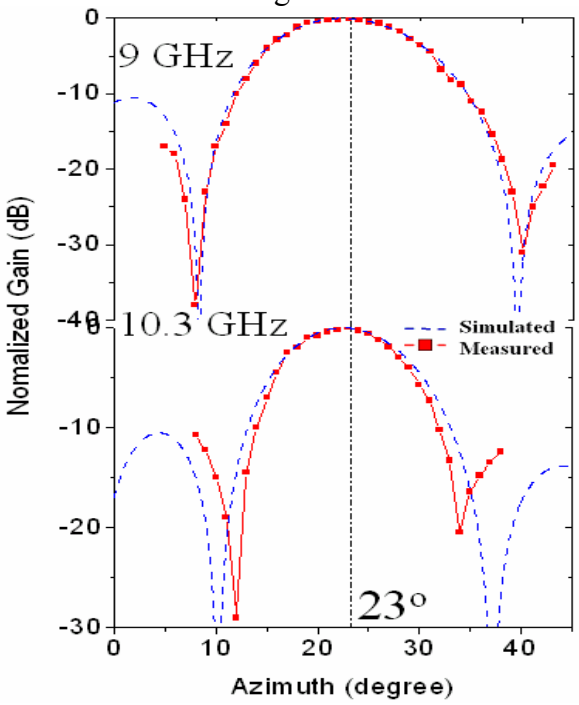
9 GHz
10.3 GHz
Simulated
Measured
23°
Nomalized Gain (dB)
Azimuth (degree)

Fig. 11

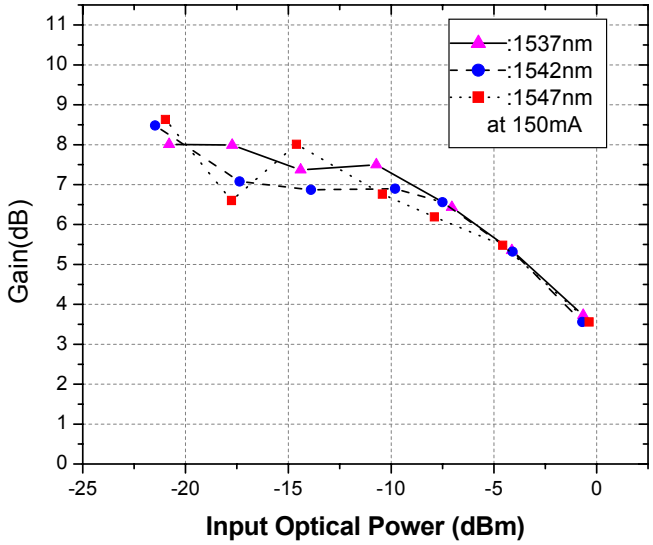


Fig. 12

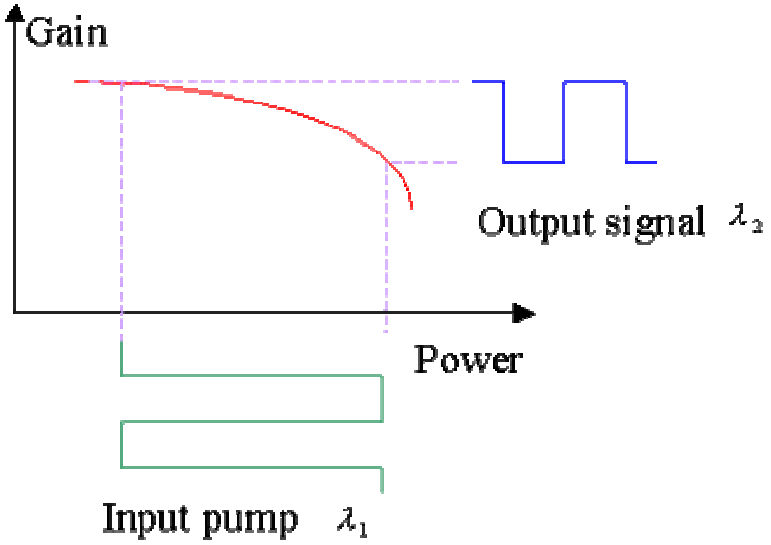


Fig. 13

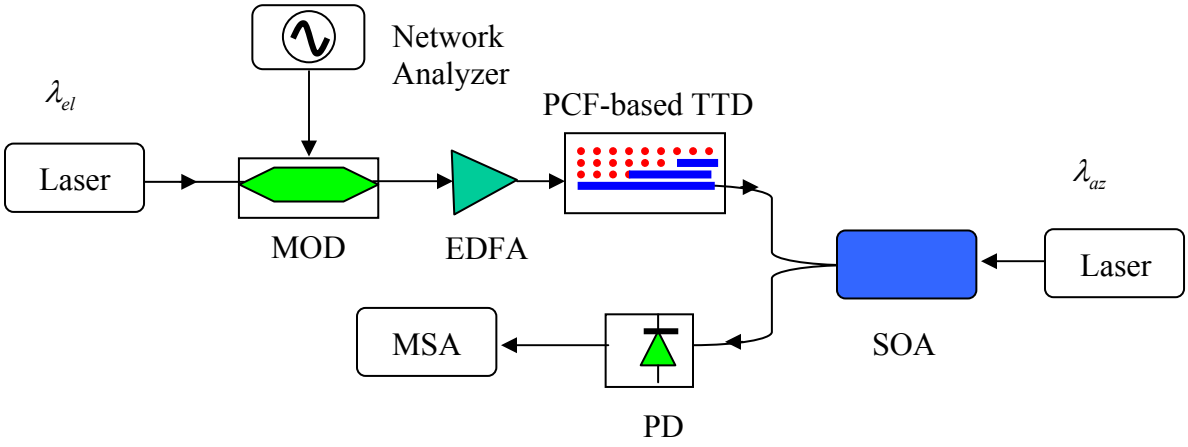


Fig. 14

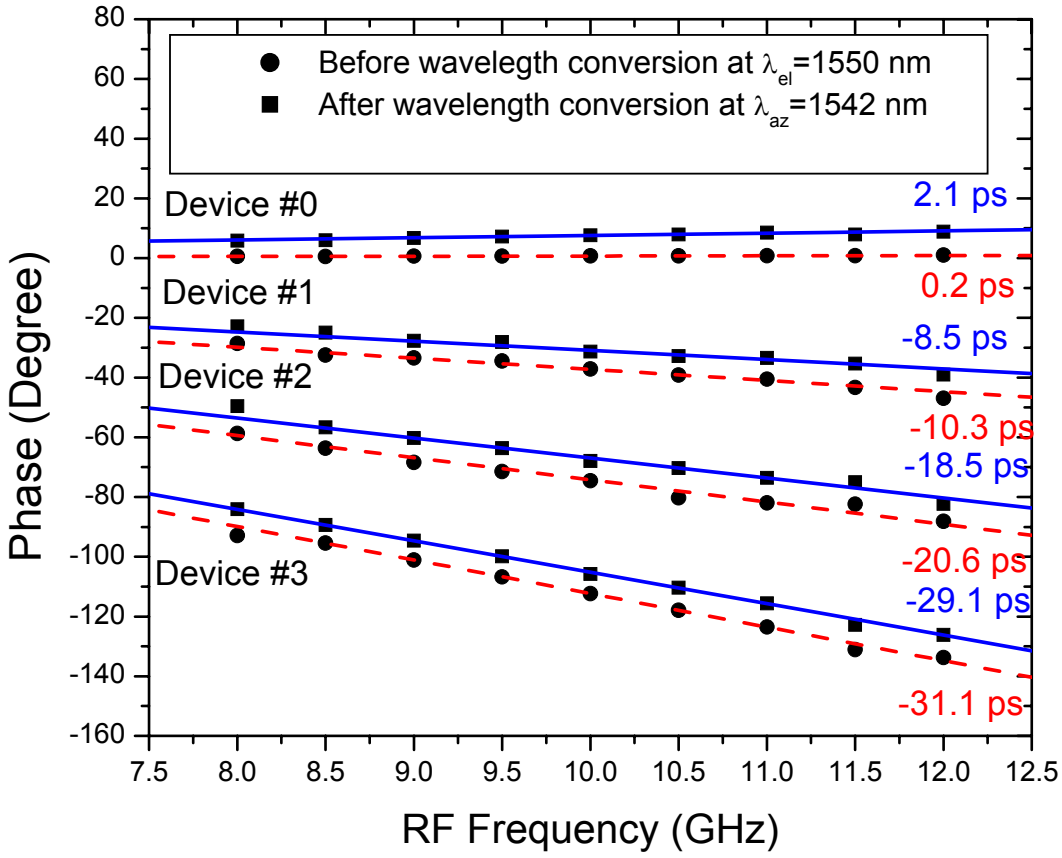
Before wavelegth conversion at λel=1550 nm
After wavelength conversion at λaz=1542 nm
Device #0
Device #1
Device #2
Device #3
2.1 ps
0.2 ps
-8.5 ps
-10.3 ps
-18.5 ps
-20.6 ps
-29.1 ps
-31.1 ps
Phase (Degree)
RF Frequency (GHz)
80
60
40
20
0
-20
-40
-60
-80
-100
-120
-140
-160
7.5
8.0
8.5
9.0
9.5
10.0
10.5
11.0
11.5
12.0
12.5

Fig. 15